Non-Covalent Functionalization of Graphene Using Self-Assembly of Alkane-Amines

*Brenda Long, Mary Manning, Micheal Burke, Bartholomaeus N. Szafranek, Giuseppe Visimberga, Damien Thompson, James C. Greer, Ian M. Povey, John MacHale, Guaylord Lejosne, Daniel Neumaier, and Aidan J. Quinn**

A simple, versatile method for non-covalent functionalization of graphene based on solution-phase assembly of alkane-amine layers is presented. Second-order Møller–Plesset (MP2) perturbation theory on a cluster model (methylamine on pyrene) yields a binding energy of ≈220 meV for the amine–graphene interaction, which is strong enough to enable formation of a stable aminodecane layer at room temperature. Atomistic molecular dynamics simulations on an assembly of 1-aminodecane molecules indicate that a self-assembled monolayer can form, with the alkane chains oriented perpendicular to the graphene basal plane. The calculated monolayer height (≈1.7 nm) is in good agreement with atomic force microscopy data acquired for graphene functionalized with 1-aminodecane, which yield a continuous layer with mean thickness ≈1.7 nm, albeit with some island defects. Raman data also confirm that self-assembly of alkane-amines is a non-covalent process, i.e., it does not perturb the sp^2 hybridization of the graphene. Passivation and adsorbate n-doping of graphene field-effect devices using 1-aminodecane, as well as high-density binding of plasmonic metal nanoparticles and seeded atomic layer deposition of inorganic dielectrics using 1,10-diaminodecane are also reported.

1. Introduction

Graphene, monolayer sheets of sp^2-hybridized carbon atoms arranged in a honeycomb-like lattice structure,[1,2] continues to attract intense research interest due to its unique electronic properties, with potential applications in nanoelectronics,[3–5] molecular electronics,[6] nanomechanics,[7–9] photonics,[10–12] sensing,[13–17] and as a candidate for (flexible) large-area transparent electrodes,[18–22] e.g., for displays and photovoltaics. As a "surface-only" nanomaterial, the properties of monolayer or few-layer graphene structures are extremely sensitive to adsorbed ambient contaminants,[23] with a correspondingly severe impact on the electrical characteristics and stability of graphene-based devices.[23–25]

Development of strategies for reproducible functionalization of graphene without adversely affecting its electronic properties is of key importance, e.g., for adsorbate doping of graphene-based devices,[1,13,26] minimizing the influence on charged impurities in the underlying substrate,[22,25,27] and also for deposition of dielectrics (via atomic layer deposition) for top-gating.[28–32] Building on scanning tunneling microscopy (STM) studies of carboxylated perylene derivatives on graphite, a number of groups have reported non-covalent functionalization strategies based on formation of self-assembled monolayers from planar 2D "tiles".[30–33] Concerning 1D molecules, STM studies of assembly of long-chain alkanes on graphite revealed stripe-like lamellar patterns, i.e., with the alkane chains lying parallel to the basal plane.[34] Formation of self-assembled monolayers on graphene from 1D "chain-like" molecules has also been reported recently. STM and atomic force microscopy (AFM) studies of long-chain alkanes (octadecanethiol and hexadecylamine) spin-cast from very dilute (<50 μM) solutions revealed formation of lamellar planar domains,[35] while a self-polymerization route has been proposed for formation of self-assembled monolayers of vertically oriented, cross-linked chains of flouroalkyltrichlorosilane.[36]

There are two main mechanisms underlying self-assembly of stable monolayers of alkane chain molecules:[37] i) the bond between the molecular "anchor" group and the substrate and ii) interchain interactions, such as van der Waals forces and, in some cases, hydrogen bonding. Concerning anchor groups, there have been several studies of interactions of ammonia molecules with the surface of graphene by monitoring charge transport in graphene field-effect devices as a function of gas exposure.[1,13,38] In their first report on graphene, Geim, Novoselov, and co-workers noted that adsorption of ammonia onto a few-layer graphene field-effect device required an anneal temperature ≈200 °C to restore the initial electrical characteristics.[1] Amine groups have also been shown to physisorb onto semiconducting carbon nanotubes.[39,40] These data suggest

Dr. B. Long, Dr. M. Manning, M. Burke, Dr. G. Visimberga, Dr. D. Thompson, Dr. J. C. Greer, Dr. I. M. Povey, J. MacHale, G. Lejosne, Dr. A. J. Quinn
Tyndall National Institute
University College Cork
Lee Maltings, Dyke Parade, Cork, Ireland
E-mail: aidan.quinn@tyndall.ie
B. N. Szafranek, Dr. D. Neumaier
Advanced Microelectronic Center Aachen (AMICA)
AMO GmbH, Otto-Blumenthal-Str. 25, 52074 Aachen, Germany

DOI: 10.1002/adfm.201101956

amines to be good candidates as anchor groups for molecular adsorbates on graphene. Finally, n-type doping of nanotubes and graphene using ammonia or molecules containing amine groups has been reported by several groups.[1,13,38,39,41]

2. Results and Discussion

2.1. Self-Assembly of Alkane-Amine Monolayers on Graphene

We report a simple, versatile method for non-covalent functionalization of the basal plane of graphene, based on solution-phase assembly of alkane-amines (**Figure 1**). Each alkane-amine molecule in the assembly can be thought of as a modular unit comprising an anchor group (*A*), a spacer group (*S*), and a terminal group (*T*). The anchor group, an amine for this study, forms a non-covalent bond to the exposed basal plane of the graphene substrate. The alkyl-chain spacer group acts to stabilize the monolayer through interchain interactions; and the terminal group provides additional functionality. Initial experiments focused on investigation of self-assembled monolayer formation using 1-aminodecane, (NH_2)–$(CH_2)_9$–(CH_3). In each experiment, the starting substrate was a Si/SiO_2 chip substrate (90 thermal oxide). The SiO_2 surface was modified prior to mechanical exfoliation of graphene by activation in oxygen plasma and immersion for 24 h in a 10 mM solution of 1,10-diaminodecane in methanol:tetrahydrofuran (1:9). This surface pre-treatment was found to improve the yield of monolayer and few-layer graphene flakes. Figure 1b,c show schematics of a typical graphene sample deposited onto a diaminodecane-functionalized SiO_2 substrate, followed by functionalization of the exposed basal plane with a layer of 1-aminodecane molecules. A series of experiments was performed to gain insight into the 1-aminodecane functionalization process. Figure 1d shows tapping-mode AFM topography data for an ≈3 μm × 3 μm multilayer region of the graphene flake shown in Figure 1a, acquired following exfoliation. Figure 1e shows AFM data acquired from the same region following solvent cleaning of the graphene-bearing chip and immersion for 2 h in a 10 mM solution of 1-aminodecane in methanol:tetrahydrofuran. Nucleation of isolated islands across the flake is evident suggesting that this immersion time (2 h) isn't sufficient for formation of a continuous layer. Figure 1g,h show AFM data for another flake following exfoliation (g) and subsequent solvent cleaning and immersion for 24 h in 1-aminodecane (h). The data in Figure 1h indicate formation of a continuous layer, together with some nanoscale islands and a number of mesoscale islands (marked 1 to 4) with heights >40 nm. Histogram analysis of these AFM data shows a mean thickness of 1.7 nm for the 1-aminodecane layer (Figure 1j).

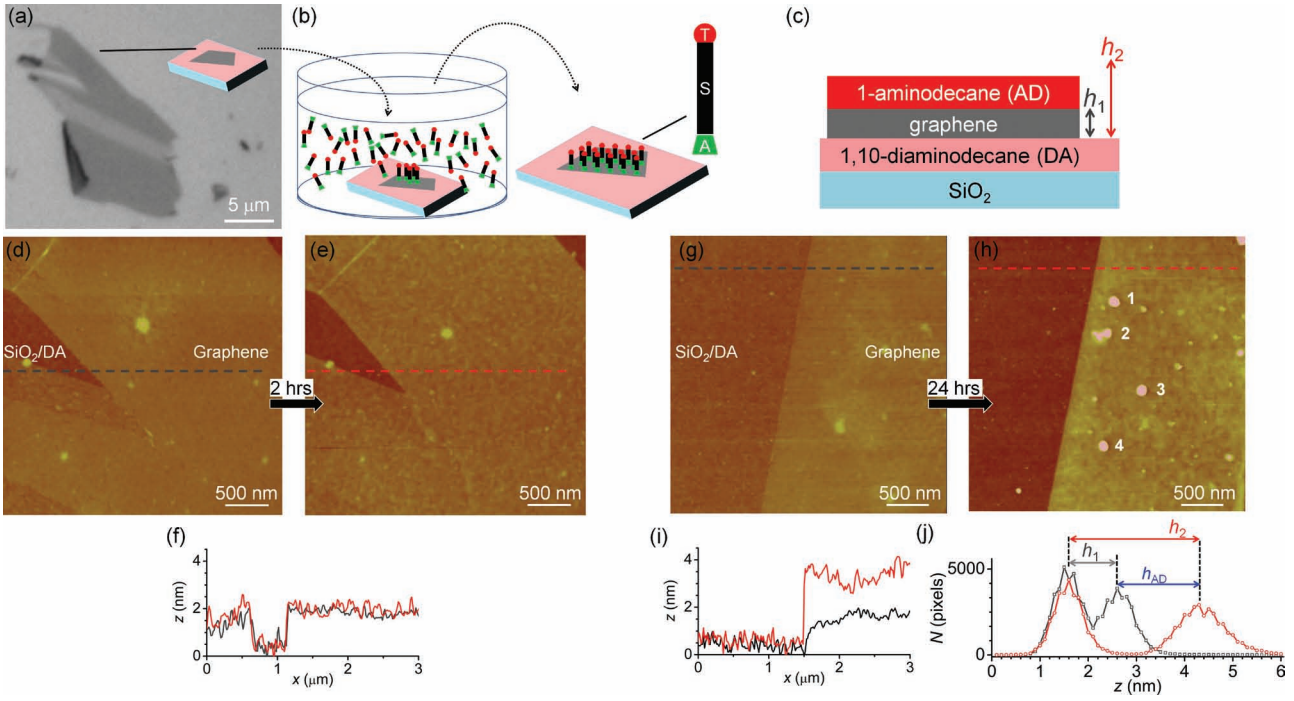

Figure 1. a) Optical image of a multilayer graphene flake mechanically exfoliated onto an oxidized silicon chip (90 nm thermal SiO_2) pre-treated with 1,10-diaminodecane. b) Schematic depicting solution-phase formation of a self-assembled monolayer of alkane-amines on the exposed basal plane of a graphene flake, where each molecule comprises an amine anchor group (*A*), an alkyl-chain spacer group (*S*), and a terminal group (*T*). c) Schematic layer stack for a graphene flake exfoliated onto diaminodecane-functionalized SiO_2 and subsequently functionalized with 1-aminodecane, (NH_2)–$(CH_2)_9$–(CH_3). d) Tapping-mode AFM topography data for an ≈3 μm × 3 μm region of the graphene flake shown in (a). e) AFM data acquired for the same region following solvent cleaning and immersion for 2 h in a 10 mM solution of 1-aminodecane in methanol:tetrahydrofuran. f) Height (*z*) vs. position (*x*) data for the dashed lines in (d,e). AFM data for another flake following exfoliation (g) and subsequent solvent cleaning and immersion for 24 h in 1-aminodecane (h). i) Height (*z*) vs position (*x*) data for the dashed lines in (g,h). j) Histogram analysis of the AFM data shown in panels (g,h) (gray and red data, respectively) yields a mean thickness for the 1-aminodecane layer, $h_{AD} \approx 1.7$ nm.

2.2. Binding of Gold Nanoparticles to Diaminodecane-Functionalized Graphene

Further functionalization experiments employed 1,10-diaminodecane, (NH_2)–$(CH_2)_{10}$–(NH_2), chosen so that the the terminal group (*T*, an amine in this case) would be available for binding of target moieties, e.g., gold nanoparticles (**Figure 2**).[42–44] As before, graphene flakes were mechanically exfoliated onto diaminodecane-modified Si/SiO_2 chips pre-patterned with micrometer-scale gold binary alignment marks (Supporting Information, Figure S1). Each graphene-bearing chip was then immersed in a solution of diaminodecane for a fixed time (2 h, 12 h, or 24 h), then subsequently immersed in a solution of citrate-stabilized gold nanoparticles (core diameter 20 nm, concentration 7×10^{11} mL^{-1}) for 6 h, and finally inspected using scanning electron microscopy (SEM).

Figure 2b–d show typical SEM images acquired at the edges of graphene flakes, one for each of the diaminodecane immersion times. Uniform binding of Au nanoparticles across the diaminodecane-functionalized SiO_2 substrate is evident in all cases, indicating a significant areal density of available amine binding groups. The assembly of closely-spaced nanoparticles, ≈600 per μm^2 on the SiO_2 region in Figure 2b, confirms mediation of the inter-nanoparticle electrostatic repulsion, which is due to the stabilizing citrate molecules at the nanoparticle surface, by the attractive interaction between each nanoparticle and the terminal amine groups in the underlying diaminodecane layer. Uniform assemblies of nanoparticles with similar areal densities were also observed on the gold binary alignment marks located across the chip, ≈580 nanoparticles per μm^2 for gold surfaces on the chip bearing the flake shown in Figure 2b.

Only a low areal density of bound nanoparticles was observed on graphene surfaces which were immersed in 10 mM diaminodecane for short periods and subsequently immersed in nanoparticle solutions. For example, Figure 2b shows results from an experiment where a short immersion time in diaminodecane (2 h) yielded a low coverage of nanoparticles, ≈95 per μm^2. Longer immersion times in diaminodecane led to higher surface densities of Au nanoparticles on diaminodecane-functionalized graphene: ≈650 per μm^2 for 12 h immersion (Figure 2c) and ≈830 per μm^2 for 24 h immersion (Figure 2d).

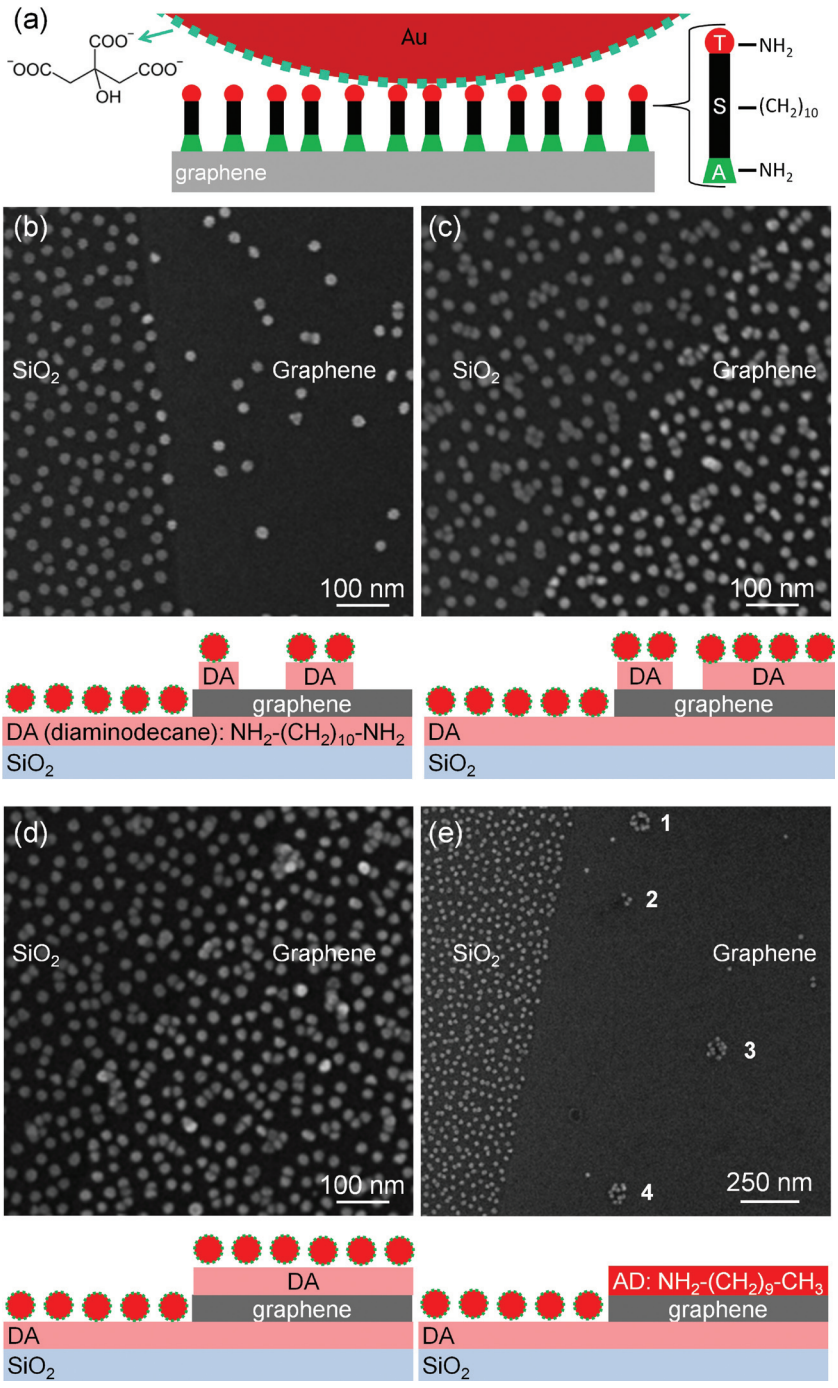

Figure 2. Binding of gold nanoparticles using 1,10-diaminodecane. a) Schematic (not to scale) depicting binding of citrate-stabilized gold nanoparticles to a graphene surface functionalized with 1,10-diaminodecane (DA). b–d) SEM images (top) and schematics (bottom) for functionalization experiments on three graphene flakes, which had been mechanically exfoliated onto separate diaminodecane-modified oxidized silicon chips. Each chip was immersed in a 10 mM solution of 1,10-diaminodecane for a fixed period (b: 2 h, c: 12 h, and d: 24 h) and subsequently immersed (6 h for each chip) in a solution of citrate-stabilized gold nanoparticles (core diameter, d = 20 nm). e) SEM image and schematic of the graphene flake shown in Figure 1h, where, following functionalization of the exposed graphene surface with 1-aminodecane (AD), the chip was immersed in a solution of d = 20 nm gold nanoparticles. The island regions marked 1–4, which show local binding of gold nanoparticles, correspond to the mesoscale islands in Figure 1h.

By contrast, functionalization of graphene with 1-aminodecane (24 h immersion) and subsequent immersion in a solution of Au nanoparticles did not result in significant binding of nanoparticles. Figure 2e shows SEM data from the same region of the aminodecane-functionalized graphene flake shown in Figure 1h, acquired following immersion in a solution of gold nanoparticles for 6 h. As before, uniform binding of nanoparticles can be observed across the diaminodecane-functionalized Si/SiO_2 substrate. However, on the aminodecane-functionalized graphene, only a very low surface density of bound nanoparticles can be observed across most of the region (≤5 per μm^2), indicating a low density of available binding groups. This observation, in conjunction with the measured height of the 1-aminodecane layer, supports our assertion that 1-aminodecane molecules can form a vertically oriented, self-assembled monolayer on graphene. We note however that this 1-aminodecane layer contains defects: the locations marked 1–4 (the mesoscale islands with heights >40 nm in the AFM data of Figure 1h) show local binding of nanoparticles, indicative of a significant number of amine binding groups on these islands, possibly arising from non-uniform (e.g., head-to-tail) local packing of the aminodecane molecules.

Thus, the interaction of assemblies of alkane-amine molecules with graphene surfaces can be employed for a variety of processes, including enhancement of the deposition yield of graphene on a target surface (e.g., SiO_2) and binding of target moieties, e.g., gold nanoparticles or nanorods for surface-enhanced Raman spectroscopy.[45] A wide variety of other functions could also be developed through selection of appropriate anchor and/or terminal groups. However, it is unlikely that the diaminodecane molecules could self-assemble as monolayers on graphene. AFM data on diaminodecane-functionalized graphene (Supporting Information, Figure S6) suggests multilayer island formation with a significant number of mesoscale islands of thickness >40 nm, possibly due to interchain amine–amine interactions that would hinder monolayer formation.

2.3. Ab Intio Calculations of Amine-Graphene Binding Energy

In order to probe the interaction mechanism between the amine anchor group and the graphene surface, ab initio calculations on a model system (methylamine above pyrene) were employed (**Figure 3**a,b). For the weak molecule-surface bond, van der Waals interactions play a critical role and approximate density functional theories are not an appropriate theoretical description. Second-order Møller–Plesset perturbation theory is a reliable and efficient post Hartree–Fock method that includes van der Waals interactions (Supporting Information, Section A). This perturbation theory is capable of describing electrostatic, inductive, and dispersive interactions, although there is a tendency to overestimate dispersion energy slightly.

From total energy calculations on the molecule-pyrene cluster and the isolated pyrene and methylamine molecules, respectively, the binding energy for the configuration depicted in Figure 3a, which we refer to as an "over-bond" site, was found to be –220 meV. Additional calculations, performed with the amine group placed directly over an atom ("over-atom" site) or over the center of one of the phenyl rings ("over-ring" site) yielded binding energies of –223 meV and –215 meV, respectively, indicating that there is no strong preferential bonding site to the graphene plane. Concerning adsorbate doping, a

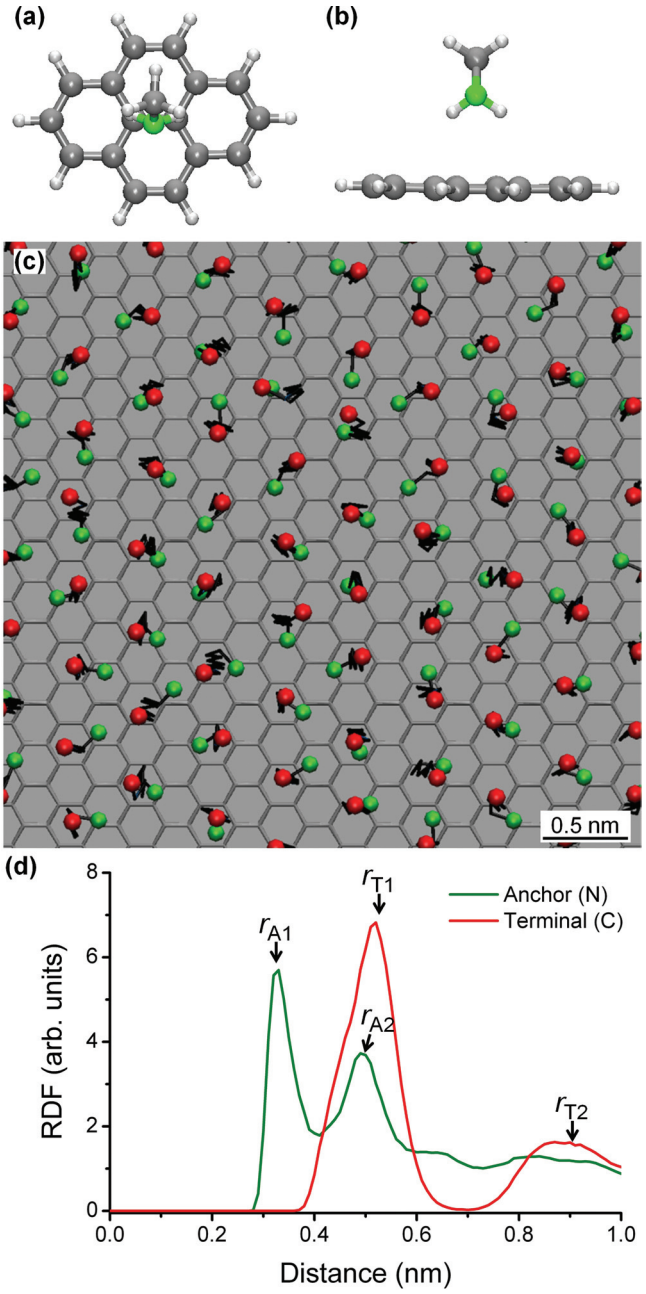

Figure 3. Top view (a) and side view (b) of the methylamine on pyrene cluster geometry, calculated using second order Møller–Plesset perturbation theory. Carbon atoms are shown in dark gray, hydrogen in light gray, and nitrogen in green. c) Top view (ball and stick representation) of the central region on the 13 nm × 15 nm graphene substrate used for the molecular dynamics simulations. For each 1-aminodecane molecule, the nitrogen atom in the amine anchor group is green, the alkane chain is black, and the carbon in the terminal methyl group is red. All hydrogen atoms are omitted for clarity. d) Radial distribution functions (RDFs) for the nitrogen atoms in the amine anchor groups (green) and the carbon atoms in the methyl terminal groups (red).

Mulliken partial charge analysis (relative to the isolated pyrene molecule) indicates a small net charge transfer with methylamine donating approximately 0.01 electron to pyrene. The calculated amine-graphene interaction (≈220 meV binding energy) is thus strong enough to enable formation of a stable aminodecane layer at room temperature.

2.4. Atomistic Molecular Dynamics Simulations of a 1-Aminodecane Monolayer on Graphene

Atomistic molecular dynamics simulations were performed to verify theoretically that the amine-graphene interaction is conducive to formation of a self-assembled monolayer (Supporting Information, Section A,C). The minimum energy configuration of an initially (laterally) compressed film comprising 784 1-aminodecane chains on a 13 nm × 15 nm monolayer graphene substrate was first found and the simulation temperature was then raised from 0 K to 295 K. The model was then subjected to 12 ns of free dynamics with no constraints on the film to allow formation of an equilibrated structure. Figure 3c shows a top view of the central region of the monolayer after 12 ns; see Supporting Information, Figure S3a for a top view of the entire substrate. Although all hydrogen atoms have been omitted for ease of viewing, it is worth noting that the monolayer is close-packed; see Supporting Information, Figure S4d for a van der Waals spheres representation of the 1-aminodecane molecules.

The nitrogen atoms of the anchor groups lie ≈0.33 nm above the graphene surface (mean value for the central 8 nm × 8 nm region), in excellent agreement with the range of values extracted from the ab initio calculations for the three non-covalent bonding configurations described above (0.315–0.33 nm). The layer height for 1-aminodecane monolayer, taken as the mean value for the vertical separation between the carbon atom in each terminal methyl group and the underlying graphene substrate over the central 8 nm × 8 nm region, is 1.7 nm with a standard deviation of 0.4 nm; see Figure S3b for an end view of the entire substrate. These results support our assertion that the region with AFM data shown in Figure 1h comprises a self-assembled monolayer of vertically oriented 1-aminodecane molecules on graphene.

Figure 3d shows the radial distribution functions (RDFs) for the nitrogen atoms in the amine anchor groups and also for the carbon atoms in the terminal methyl groups, calculated over the central 8 nm × 8 nm region. The positions of the first and second RDF peaks for the anchor nitrogen atoms, r_{A1} = 0.33 nm and r_{A2} = 0.49 nm, correspond to the nearest- and next-nearest-neighbor separations, respectively. The ratio, $r_{A2}/r_{A1} \approx 1.48$, which is smaller than the value for a perfect hexagonal lattice ($\sqrt{3} \approx 1.73$), indicates significant deviations from hexagonal packing, likely due to local amine–amine interactions between neighboring anchor groups. By contrast, the positions of the RDF peaks for the terminal carbon atoms, r_{T1} = 0.52 nm, r_{T2} = 0.89 nm ($r_{T2}/r_{T1} \approx 1.71$), indicate quasi-hexagonal packing. Figure 3d also shows that there is no significant overlap between the first RDF peaks for the anchor nitrogens and the terminal carbons. This may result from coupled precession of the terminal methyl groups on neighboring aminodecane molecules around the respective anchoring amines. The simulations also reveal collective random-walk type displacements of the anchor amine groups, with root-mean-square displacements of the nitrogen atoms ≈0.12 nm over the last 2 ns of free dynamics (Supporting Information, Section C and also the corresponding movies). Thus, the molecular dynamics

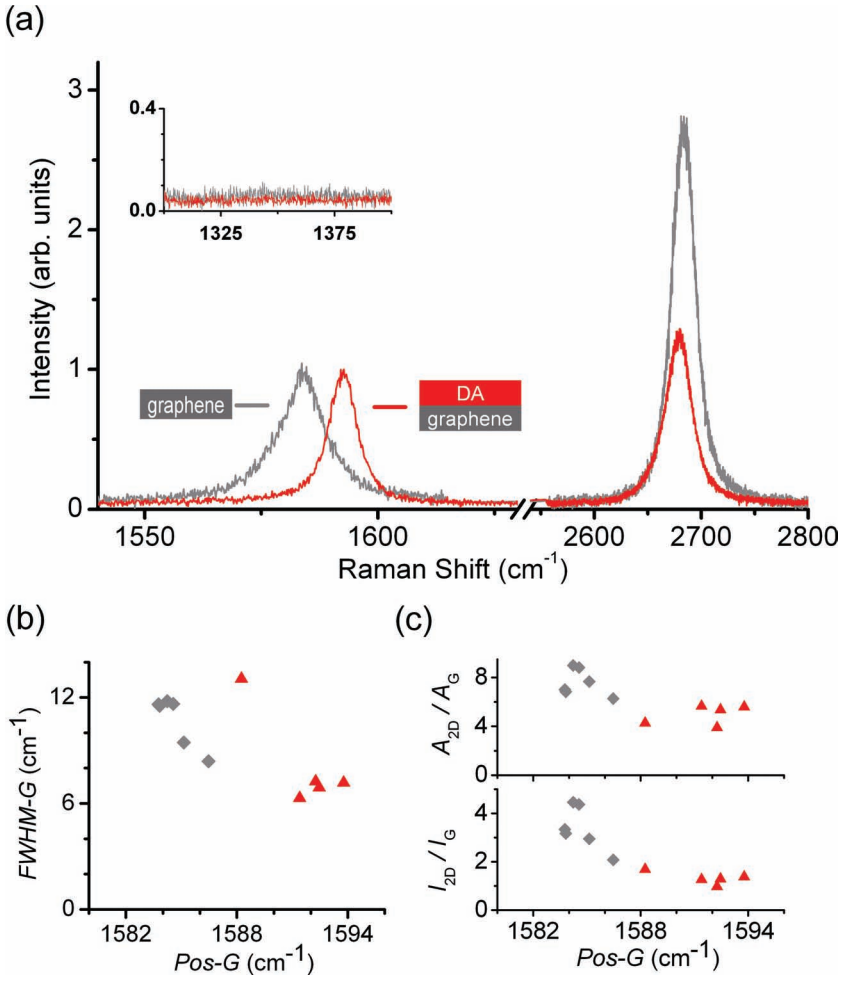

Figure 4. Raman spectra for a graphene monolayer deposited onto an unmodified Si/SiO_2 substrate (gray) and also for a graphene monolayer (red) following following functionalization in solution with 1,10-diaminodecane. All data were acquired at 514.5 nm excitation and each spectrum was normalized to the maximum of the G peak. Inset: No defect (D) peak ≈ 1350 cm^{-1} is observed following functionalization. b,c) FWHM for the G peak (FWHM-G); frequency-integrated area ratio of the 2D and G peaks (A_{2D}/A_G) and peak height ratio (I_{2D}/I_G), plotted versus the position of the G peak (Pos-G) for unmodified monolayer graphene (gray diamonds) and graphene functionalized with 1,10-diaminodecane (red triangles).

simulations indicate formation of a mobile but stable self-assembled monolayer on graphene, consistent with the amine-graphene binding energy predicted by the ab initio calculations and the AFM data presented in Figure 1.

2.5. Raman Spectroscopy on Functionalized Graphene

Measured Raman spectroscopy data for graphene monolayers functionalized with 1,10-diaminodecane (**Figure 4**, red data) are also consistent with a non-covalent, charge-transfer interaction between the layer of alkane-amine molecules and the graphene surface. The peak close to 2680 cm^{-1} (two-phonon 2D band) with full width at half-maximum intensity (FWHM) ≈24.5 cm^{-1} is characteristic of monolayer graphene.[46] Furthermore, the absence of a peak close to 1350 cm^{-1} (defect D band) following functionalization (Figure 4, inset) confirms that the layer of

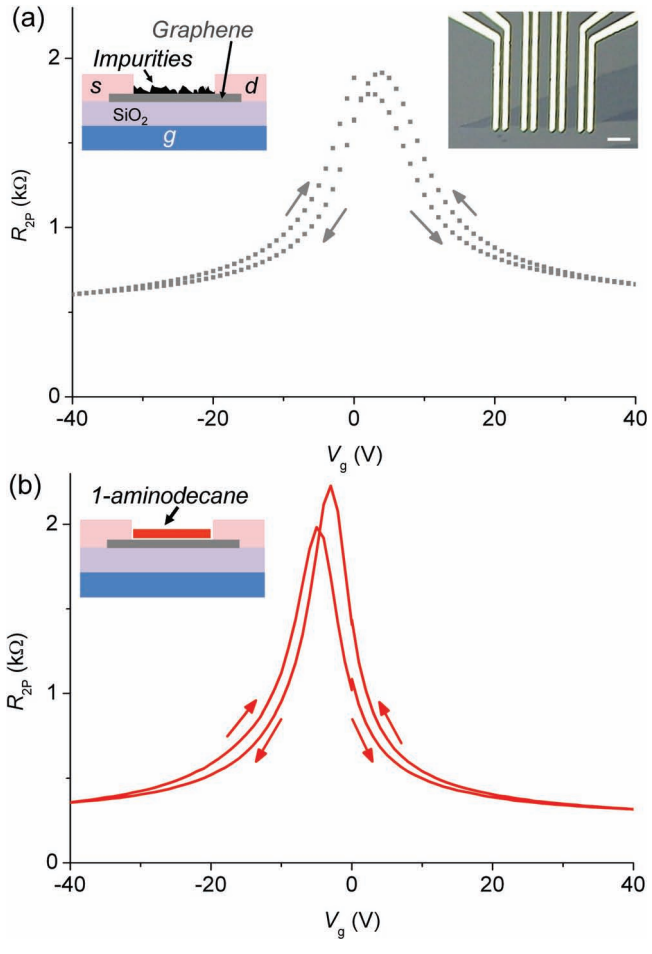

Figure 5. Carrier transport in functionalized graphene monolayers. a) Two-probe resistance vs. gate-voltage (R_{2P}–V_g) characteristics measured in vacuum for a back-gated, monolayer graphene device following fabrication. For each measurement, the drain bias was held at 20 mV and the gate voltage was swept from 0V → 40 V → –40 V → 0 V, as indicated by the gray arrows. Insets: Schematic and optical microscopy image of an as-fabricated monolayer graphene device (scale bar: 10 µm). b) R_{2P}–V_g characteristics for the device with data is shown in (a) following thermal annealing and functionalization in solution with 1-aminodecane.

1,10-diaminodecane molecules does not significantly perturb the sp^2 hybridization of the graphene monolayer and does not introduce additional structural defects.

The spectrum for the functionalized monolayer shows several significant differences when compared with data measured for an as-deposited graphene monolayer on an unmodified SiO_2 substrate (Figure 4, gray data). Both the shift in the position of the *G* peak (centered close to 1580 cm^{-1}) towards higher energy and the reduction in intensity of the 2D peak following functionalization of the exposed graphene surface with 1,10-diaminodecane are consistent with doping,[47–50] likely via charge transfer.[27,38,51]

Figure 4b,c summarize the results extracted from a larger sample set of graphene monolayers. None of spectra showed a defect (D) peak. For unmodified graphene, the range of values for the the FWHM of the G peak (FWHM-G), plotted as a function of the G peak position (Pos-G), agrees well with published data on unmodified monolayer graphene flakes and indicate moderate surface doping, likely due to adsorbed contaminants.[52] For diaminodecane-functionalized graphene, all flakes show higher values of Pos-G and four of the five data points show small values for FWHM-G (≈7 cm^{-1}), consistent with carrier concentrations ≈10^{12} cm^{-2} (ref. [47,50]), likely from charge transfer from the diaminodecane adsorbate dopants.

Figure 4c shows the extracted values for the ratio of the frequency-integrated areas under the 2D and G peaks (A_{2D}/A_G) and the ratio of the peak heights (I_{2D}/I_G). For monolayer graphene, no significant dependence of A_G on doping is expected,[53] while A_{2D} is inversely proportional to the square of the electron (or hole) scattering rate.[54] Both ratios (A_{2D}/A_G and I_{2D}/I_G) are maximum for zero doping and decrease with increasing doping. The data presented in Figure 3c indicate moderate surface doping from charged impurities for the as-deposited graphene, A_{2D}/A_G ≈ 6–9 and I_{2D}/I_G ≈ 2–5, while the corresponding values for the diaminodecane-modified graphene, A_{2D}/A_G ≈ 4–6 and I_{2D}/I_G ≈ 1–2, are consistent with significant adsorbate doping, ≈10^{12} cm^{-2}, likely due to charge transfer from the amine groups in the diaminodecane layer.

2.6. Functionalized Graphene Field-Effect Devices

As described earlier, minimizing scattering from adsorbed ambient contaminants is a significant challenge for development of graphene-based electronic devices. We have investigated the self-assembly of 1-aminodecane molecules as a potential route for passivating graphene field-effect devices (**Figure 5**). Figure 5a shows two-probe resistance (R_{2P}) versus gate voltage (V_g) data measured in vacuum for a monolayer graphene field-effect device fabricated on an unmodified SiO_2 substrate. The data show the expected behavior for unpassivated graphene devices exposed to ambient conditions–hysteretic ambipolar conduction, with minimum conductivity (Dirac point) at positive gate voltages, $V_{g,DP}$ ≈ 2 V, 4 V, respectively, for the two peaks in the double sweep measurement. A positive value for $V_{g,DP}$ indicates (unintentional) hole doping, likely from contaminants at the graphene surface and the graphene-substrate interface, e.g., adsorbed water, oxygen, and organic

residue from the fabrication process.[13,23,25,27] Hysteretic behavior has been attributed to the presence of dipolar adsorbates,[23,25,27] and charge traps at the graphene/SiO_2 interface.[51] Figure 5b shows the R_{2P}–V_g data for the same device acquired following annealing to 200 °C under nitrogen for 1 h, functionalization in solution with 1-aminodecane and transfer under ambient conditions (≈1 h) to the vacuum measurement chamber. Several significant changes are evident, including a shift in the Dirac point to negative gate voltage ($V_{g,DP}$ ≈ –3 V, –5 V) and a sharper resistance peak (higher carrier mobility) around the Dirac point for each sweep, relative to the R_{2P}–V_g data for the as-fabricated device. These negative values for the Dirac point in the functionalized device indicate adsorbate-induced electron doping, presumably from the amine anchor groups in the 1-aminodecane molecular layer.[1,13,25,29] Neglecting quantum capacitance effects, the two-probe Drude mobility, μ, can be estimated using

$$\mu = \frac{1}{R_{2P}} \frac{L}{W} \frac{t_{ox}}{\varepsilon_0 \varepsilon_r |V_g - V_{g,DP}|}$$

where L (≈ 6 μm) and W (≈ 10 μm) are the device length and width, respectively; ε_0 is the permittivity of free space; and ε_r (3.9) and t_{ox} (90 nm) are the relative permittivity and thickness of the SiO_2 dielectric, respectively. Analysis of the data in Figure 4b leads to values of μ_e ≈ 3000–3100 $cm^2\ V^{-1}\ s^{-1}$ for the electron mobility and μ_h ≈ 2400–2500 $cm^2\ V^{-1}\ s^{-1}$ for the hole mobility at a gate-induced carrier density of 1.2 × 10^{12} cm^{-2}. In general, devices functionalized with 1-aminodecane following annealing yielded higher carrier mobilities and also improved stability upon re-exposure to ambient conditions compared with annealed "bare" devices, suggesting that the 1-aminodecane layer can act as a barrier to hinder the readsorption of ambient contaminants. Devices functionalized with 1-aminodecane yielded Dirac point values in the range –5 V ≥ $V_{g,DP}$ ≥ –20 V, corresponding to (net) n-type dopant densities ≈ 1–4 × 10^{12} cm^{-2}. This range is consistent with the maximum dopant density estimate that can be extracted from the ab initio calculations and molecular dynamics simulations presented in Figure 3, ≈5 ×10^{12} cm^{-2}, based on a charge transfer of 0.01 electrons per amine anchor group and a (maximum) amine surface density ≈5 × 10^{14} cm^{-2}. Future work will focus on optimization of the solvent cleaning and thermal annealing steps[55] in order to minimize the levels of surface contaminants present prior to functionalization. Such contaminants can act as scattering centres and could also lead to defects in the alkane-amine functionalization layer.

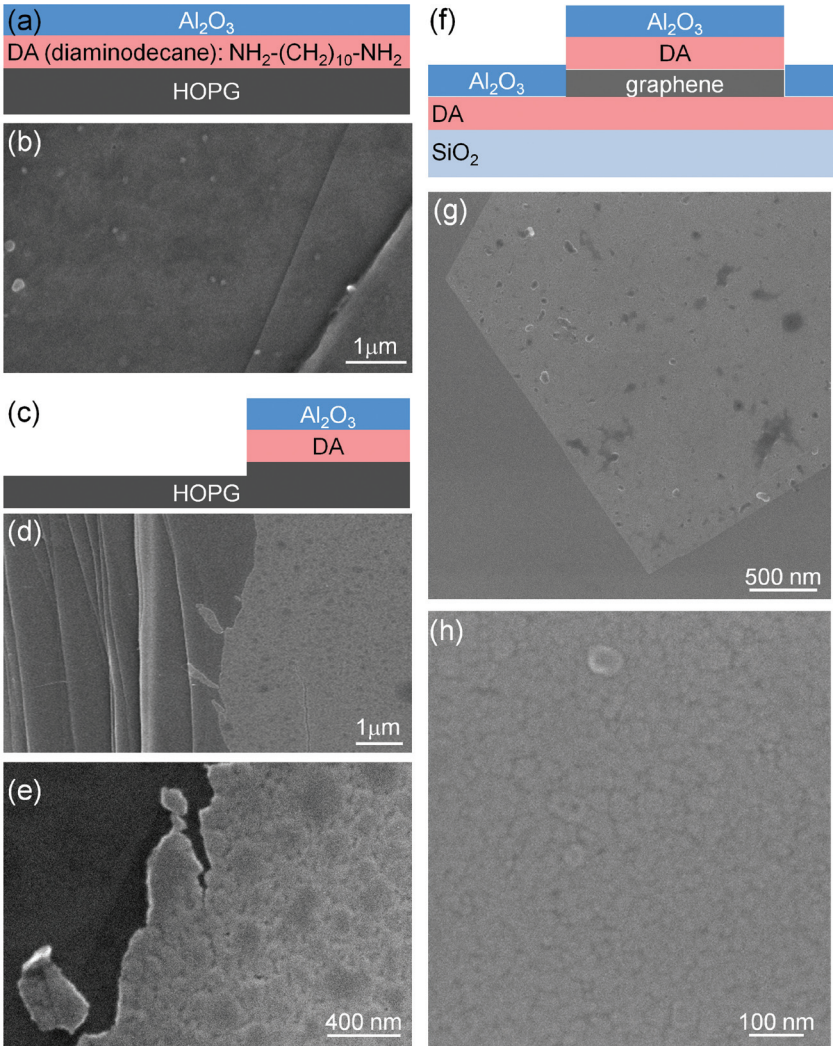

Figure 6. ALD of aluminum oxide onto diaminodecane-modified graphite and graphene. Schematic (a) and SEM image (b) of a micrometer-scale region of a HOPG substrate following functionalization with 1,10-diaminodecane and subsequent ALD of aluminium oxide (5 nm nominal thickness). Schematic (c) and SEM images (d,e) of the edge of the aluminum oxide film, following removal of part of the layer (and part of the underlying graphite) using adhesive tape. Schematic (f) and SEM images (g,h) of a diaminodecane-functionalized graphene layer following ALD of aluminium oxide (10 nm nominal thickness).

2.7. Atomic Layer Deposition of Alumina onto Functionalized Graphene

A key challenge in the development of graphene-based nanoelectronics is the deposition of inorganic dielectrics onto graphene for top- or dual-gate devices. A number of groups have developed "seeding" processes for atomic layer deposition (ALD) of inorganic dielectrics onto graphene, including ozone pre-treatment,[31,32] deposition of thin (≈10 nm) polymer layers containing appropriate binding groups,[28,56] or self-assembled monolayers of 2D perylene derivatives.[30] Such processes are necessary since conformal growth of dielectrics on bare graphene is hindered by the chemical inertia of the substrate.[30,31] Use of self-assembled alkane-amine layers represents an attractive complementary process for seeded ALD (**Figure 6**);

see Supporting Information, Section A for methods. Figure 6b shows a SEM image of an ultrathin film of aluminum oxide (5 nm nominal thickness), which was deposited onto highly oriented pyrolytic graphite (HOPG) that had been functionalized with 1,10-diaminodecane. Uniform coverage of the substrate (including some small defects and a step edge) is evident. By contrast, atomic layer deposition of aluminum oxide on freshly cleaved HOPG yielded non-uniform stripe-like structures, consistent with growth at step edges and defects only.[30]

Figure 6d shows the edge of the aluminum oxide film with SEM data shown in Figure 6b, following removal of part of the film using adhesive tape. The remaining aluminum oxide shows good adhesion to the substrate. Higher magnification images (Figure 6e) show a quasi-continuous film arising from coalescence of 2D islands, as expected for the chosen film thickness.[31,32] Similar growth was observed for ALD of aluminum oxide onto diaminodecane-functionalized graphene (Figure 6g,h). As noted earlier, the diaminodecane layer does not form a monolayer and contains a significant number of mesoscale islands (see Supporting Information, Figure S5 for AFM data).

3. Conclusions

In conclusion, self-assembly of alkane-amines represents a versatile new route for non-covalent functionalization of graphene without adversely affecting its unique properties. Advantages include adsorbate doping and surface passivation of graphene field-effect devices through choice of appropriate anchor groups. Selection of suitable terminal groups for dielectric deposition or for binding of target species onto graphene (either directly or via a secondary linker) offer routes to integrated nanoelectronic devices based on graphene, as well as graphene-based electromechanical or electrochemical (bio)sensors.

Supporting Information

Supporting Information is available from the Wiley Online Library or from the author. It includes sections A) materials and methods, B) nanoparticle binding to functionalized graphene, C) atomistic molecular dynamics simulations (including movies), and D) atomic layer deposition.

Acknowledgements

The authors acknowledge fabrication support from the engineers at Tyndall's Central Fabrication Facility, in particular Dan O'Connell. This work was supported by the European Commission under the FP7 ICT project "GRAND" (215572) and by the Irish Higher Education Authority PRTLI programmes (Cycle 3 "Nanoscience" and Cycle 4 "INSPIRE").

Received: August 19, 2011
Revised: November 3, 2011
Published online: December 16, 2011

[1] K. S. Novoselov, A. K. Geim, S. V. Morozov, D. Jiang, Y. Zhang, S. V. Dubonos, I. V. Grigorieva, A. A. Firsov, *Science* **2004**, *306*, 666.
[2] C. Berger, Z. M. Song, T. B. Li, X. B. Li, A. Y. Ogbazghi, R. Feng, Z. T. Dai, A. N. Marchenkov, E. H. Conrad, P. N. First, W. A. de Heer, *J. Phys. Chem. B* **2004**, *108*, 19912.
[3] Y. M. Lin, K. A. Jenkins, A. Valdes-Garcia, J. P. Small, D. B. Farmer, P. Avouris, *Nano Lett.* **2009**, *9*, 422.
[4] M. Sprinkle, M. Ruan, Y. Hu, J. Hankinson, M. Rubio-Roy, B. Zhang, X. Wu, C. Berger, W. A. de Heer, *Nat. Nanotechnol.* **2010**, *5*, 727.
[5] F. Schwierz, *Nat. Nanotechnol.* **2010**, *5*, 487.
[6] G. Wang, Y. Kim, M. Choe, T. W. Kim, T. Lee, *Adv. Mater.* **2011**, *23*, 755.
[7] J. S. Bunch, A. M. van der Zande, S. S. Verbridge, I. W. Frank, D. M. Tanenbaum, J. M. Parpia, H. G. Craighead, P. L. McEuen, *Science* **2007**, *315*, 490.
[8] C. Y. Chen, S. Rosenblatt, K. I. Bolotin, W. Kalb, P. Kim, I. Kymissis, H. L. Stormer, T. F. Heinz, J. Hone, *Nat. Nanotechnol.* **2009**, *4*, 861.
[9] R. A. Barton, B. Ilic, A. M. van der Zande, W. S. Whitney, P. L. McEuen, J. M. Parpia, H. G. Craighead, *Nano Lett.* **2011**, *11*, 1232.
[10] F. Xia, T. Mueller, Y.-m. Lin, A. Valdes-Garcia, P. Avouris, *Nat. Nanotechnol.* **2009**, *4*, 839.
[11] F. Bonaccorso, Z. Sun, T. Hasan, A. C. Ferrari, *Nat. Photonics* **2010**, *4*, 611.
[12] Z. P. Sun, T. Hasan, F. Torrisi, D. Popa, G. Privitera, F. Q. Wang, F. Bonaccorso, D. M. Basko, A. C. Ferrari, *ACS Nano* **2010**, *4*, 803.
[13] F. Schedin, A. K. Geim, S. V. Morozov, E. W. Hill, P. Blake, M. I. Katsnelson, K. S. Novoselov, *Nat. Mater.* **2007**, *6*, 652.
[14] P. K. Ang, W. Chen, A. T. S. Wee, K. P. Loh, *J. Am. Chem. Soc.* **2008**, *130*, 14392.
[15] X. C. Dong, Y. M. Shi, W. Huang, P. Chen, L. J. Li, *Adv. Mater.* **2010**, *22*, 1649.
[16] S. Lara-Avila, K. Moth-Poulsen, R. Yakimova, T. Bjornholm, V. Fal'ko, A. Tzalenchuk, S. Kubatkin, *Adv. Mater.* **2011**, *23*, 878.
[17] W. Li, C. Tan, M. A. Lowe, H. D. Abruna, D. C. Ralph, *ACS Nano* **2011**, *5*, 2264.
[18] X. Li, W. Cai, J. An, S. Kim, J. Nah, D. Yang, R. Piner, A. Velamakanni, I. Jung, E. Tutuc, S. K. Banerjee, L. Colombo, R. S. Ruoff, *Science* **2009**, *324*, 1312.
[19] X. M. Li, H. W. Zhu, K. L. Wang, A. Y. Cao, J. Q. Wei, C. Y. Li, Y. Jia, Z. Li, X. Li, D. H. Wu, *Adv. Mater.* **2010**, *22*, 2743.
[20] S. Bae, H. Kim, Y. Lee, X. Xu, J.-S. Park, Y. Zheng, J. Balakrishnan, T. Lei, H. R. Kim, Y. I. Song, Y.-J. Kim, K. S. Kim, B. Ozyilmaz, J.-H. Ahn, B. H. Hong, S. Iijima, *Nat. Nanotechnol.* **2010**, *5*, 574.
[21] W. H. Lee, J. Park, S. H. Sim, S. B. Jo, K. S. Kim, B. H. Hong, K. Cho, *Adv. Mater.* **2011**, *23*, 1752.
[22] W. H. Lee, J. Park, Y. Kim, K. S. Kim, B. H. Hong, K. Cho, *Adv. Mater.* **2011**, *23*, 3460.
[23] P. L. Levesque, S. S. Sabri, C. M. Aguirre, J. Guillemette, M. Siaj, P. Desjardins, T. Szkopek, R. Martel, *Nano Lett.* **2011**, *11*, 132.
[24] P. Blake, R. Yang, S. V. Morozov, F. Schedin, L. A. Ponomarenko, A. A. Zhukov, R. R. Nair, I. V. Grigorieva, K. S. Novoselov, A. K. Geim, *Solid State Commun.* **2009**, *149*, 1068.
[25] T. Lohmann, K. von Klitzing, J. H. Smet, *Nano Lett.* **2009**, *9*, 1973.
[26] W. Chen, S. Chen, D. C. Qi, X. Y. Gao, A. T. S. Wee, *J. Am. Chem. Soc.* **2007**, *129*, 10418.
[27] M. Lafkioti, B. Krauss, T. Lohmann, U. Zschieschang, H. Klauk, K. von Klitzing, J. H. Smet, *Nano Lett.* **2010**, *10*, 1149.
[28] D. B. Farmer, H. Y. Chiu, Y. M. Lin, K. A. Jenkins, F. N. Xia, P. Avouris, *Nano Lett.* **2009**, *9*, 4474.
[29] D. B. Farmer, R. Golizadeh-Mojarad, V. Perebeinos, Y. M. Lin, G. S. Tulevski, J. C. Tsang, P. Avouris, *Nano Lett.* **2009**, *9*, 388.
[30] X. R. Wang, S. M. Tabakman, H. J. Dai, *J. Am. Chem. Soc.* **2008**, *130*, 8152.
[31] B. K. Lee, S. Y. Park, H. C. Kim, K. Cho, E. M. Vogel, M. J. Kim, R. M. Wallace, J. Y. Kim, *Appl. Phys. Lett.* **2008**, *92*, 203102.

[32] B. Lee, G. Mordi, M. J. Kim, Y. J. Chabal, E. M. Vogel, R. M. Wallace, K. J. Cho, L. Colombo, J. Kim, *Appl. Phys. Lett.* **2010**, *97*, 043107.
[33] Q. H. Wang, M. C. Hersam, *Nat. Chem.* **2009**, *1*, 206.
[34] J. P. Rabe, S. Buchholz, *Science* **1991**, *253*, 424.
[35] T. Zhang, Z. G. Cheng, Y. B. Wang, Z. J. Li, C. X. Wang, Y. B. Li, Y. Fang, *Nano Lett.* **2010**, *10*, 4738.
[36] B. Lee, Y. Chen, F. Duerr, D. Mastrogiovanni, E. Garfunkel, E. Y. Andrei, V. Podzorov, *Nano Lett.* **2010**, *10*, 2427.
[37] J. C. Love, L. A. Estroff, J. K. Kriebel, R. G. Nuzzo, G. M. Whitesides, *Chem. Rev.* **2005**, *105*, 1103.
[38] X. R. Wang, X. L. Li, L. Zhang, Y. Yoon, P. K. Weber, H. L. Wang, J. Guo, H. J. Dai, *Science* **2009**, *324*, 768.
[39] J. Kong, H. J. Dai, *J. Phys. Chem. B* **2001**, *105*, 2890.
[40] D. Chattopadhyay, L. Galeska, F. Papadimitrakopoulos, *J. Am. Chem. Soc.* **2003**, *125*, 3370.
[41] M. Shim, A. Javey, N. W. S. Kam, H. J. Dai, *J. Am. Chem. Soc.* **2001**, *123*, 11512.
[42] K. C. Grabar, R. G. Freeman, M. B. Hommer, M. J. Natan, *Anal. Chem.* **1995**, *67*, 735.
[43] A. Kumar, S. Mandal, P. R. Selvakannan, R. Pasricha, A. B. Mandale, M. Sastry, *Langmuir* **2003**, *19*, 6277.
[44] L. Venkataraman, J. E. Klare, I. W. Tam, C. Nuckolls, M. S. Hybertsen, M. L. Steigerwald, *Nano Lett.* **2006**, *6*, 458.
[45] F. Schedin, E. Lidorikis, A. Lombardo, V. G. Kravets, A. K. Geim, A. N. Grigorenko, K. S. Novoselov, A. C. Ferrari, *ACS Nano* **2010**, *4*, 5617.
[46] A. C. Ferrari, J. C. Meyer, V. Scardaci, C. Casiraghi, M. Lazzeri, F. Mauri, S. Piscanec, D. Jiang, K. S. Novoselov, S. Roth, A. K. Geim, *Phys. Rev. Lett.* **2006**, *97*, 187401.
[47] S. Pisana, M. Lazzeri, C. Casiraghi, K. S. Novoselov, A. K. Geim, A. C. Ferrari, F. Mauri, *Nat. Mater.* **2007**, *6*, 198.
[48] J. Yan, Y. B. Zhang, P. Kim, A. Pinczuk, *Phys. Rev. Lett.* **2007**, *98*, 166802.
[49] J. Yan, Y. B. Zhang, S. Goler, P. Kim, A. Pinczuk, *Solid State Commun.* **2007**, *143*, 39.
[50] A. Das, S. Pisana, B. Chakraborty, S. Piscanec, S. K. Saha, U. V. Waghmare, K. S. Novoselov, H. R. Krishnamurthy, A. K. Geim, A. C. Ferrari, A. K. Sood, *Nat. Nanotechnol.* **2008**, *3*, 210.
[51] J. S. Lee, S. Ryu, K. Yoo, I. S. Choi, W. S. Yun, J. Kim, *J. Phys. Chem. C* **2007**, *111*, 12504.
[52] C. Casiraghi, S. Pisana, K. S. Novoselov, A. K. Geim, A. C. Ferrari, *Appl. Phys. Lett.* **2007**, *91*, 233108.
[53] D. M. Basko, S. Piscanec, A. C. Ferrari, *Phys. Rev. B* **2009**, *80*, 165413.
[54] D. M. Basko, *Phys. Rev. B* **2008**, *78*, 125418.
[55] Z. G. Cheng, Q. Y. Zhou, C. X. Wang, Q. A. Li, C. Wang, Y. Fang, *Nano Lett.* **2011**, *11*, 767.
[56] F. N. Xia, D. B. Farmer, Y. M. Lin, P. Avouris, *Nano Lett.* **2010**, *10*, 715.